#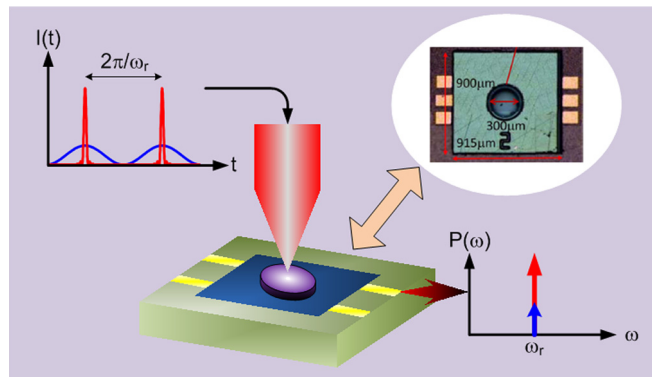 Spectral Power Enhancement in a 100 GHz Photonic Millimeter-Wave Generator Enabled by Spectral Line-by-Line Pulse Shaping

F.-M. Kuo
J.-W. Shi
H.-C. Chiang
H.-P. Chuang
H.-K. Chiou
C.-L. Pan
N.-W. Chen
H.-J. Tsai
C.-B. Huang

Spectral Power Enhancement in a 100 GHz Photonic Millimeter-Wave Generator Enabled by Spectral Line-by-Line Pulse Shaping

F.-M. Kuo,[1] **J.-W. Shi,**[1] **H.-C. Chiang,**[2] **H.-P. Chuang,**[2] **H.-K. Chiou,**[1] **C.-L. Pan,**[2,3] **N.-W. Chen,**[4] **H.-J. Tsai,**[1] **and C.-B. Huang**[2]

[1]Department of Electrical Engineering, National Central University, Taoyuan 320, Taiwan
[2]Institute of Photonics Technologies, National Tsing-Hua University, Hsinchu 300, Taiwan
[3]Department of Physics, National Tsing-Hua University, Hsinchu 300, Taiwan
[4]Department of Communications Engineering, Yuan Ze University, Zhongli 320, Taiwan

Abstract: We report generation of high-modulation-depth photonic millimeter-wave (MMW) waveforms by applying line-by-line pulse shaping on a phase-modulated continuous-wave frequency comb. The optimized 20 and 100 GHz optical waveforms are then converted into electrical MMW signals using a near-ballistic uni-traveling-carrier photodiode (NBUTC-PD). A 7.4 dB MMW power enhancement is experimentally achieved by using 2.6 ps optimized pulses at a 100 GHz repetition rate, as compared with excitation by a conventional sinusoidal signal for the NBUTC-PD operated at the same photocurrent. This is in qualitative agreement with a theoretical analysis of spectral power enhancement by optical short pulses comprised of equi-amplitude frequency lines over sinusoidal excitation.

Index Terms: Microwave photonics signal, optical communications, photodetectors, pulse shaping.

1. Introduction

Microwave and millimeter-wave (MMW) photonics have recently attracted immense research attention [1]–[3]. Optical pulse-shaping techniques [4], [5] have also been found to be extremely useful for generation of arbitrary ultrawideband and radio-frequency (RF) signals [6]–[11]. Optical line-by-line pulse shaping [12] combines the functionality of conventional pulse shaping with the high-frequency stability and long-term temporal coherence of an optical frequency comb [13]. With the amplitude and phase of each frequency comb line independently controlled, line-by-line shaped waveforms can span the entire time-domain comb repetition period, thus enabling optical arbitrary waveform generation [14], [15]. Line-by-line pulse shaping with added time-multiplexing functionality has also been used to demonstrate rapid reprogrammable arbitrary microwave waveform generation [16] as well as the tailoring of microwave power spectra [17], [18].

Limited by the electrical bandwidth of commercially available photodetectors (PDs), the aforementioned demonstrations of shaper-assisted microwave photonics have been focused on frequency ranges below 60 GHz. It would be extremely attractive to extend the frequency range of

microwave photonics by using PDs with larger electrical bandwidths. This endeavor also meets the growing demand of gigabit wireless access applications [19], as well as radio-over-fiber communication systems [20], [21]. MMW carriers in the W-band (75–110 GHz) or above are of particular interests. Compared with the unlicensed V-band (60 GHz) [22], the W-band exhibits a much broader window of minimum propagation loss and is thus more suitable for the application to outdoor gigabit wireless Ethernet in the near future [19].

The coverage area of each base station in a W-band wireless system is limited by the relatively higher propagation loss of W-band signal than that of RF bands in free space. As a result, the optical MMW signal is typically generated at the central office and is only converted into electrical form at the last mile in base stations using high-speed/power PDs [20], [21]. To provide longer lifetime and higher reliability of these delicate high-speed PDs, an optical MMW waveform with high modulation depth (e.g., optical short pulses) is more desirable than conventional optical sinusoidal excitation [23]. This is due to the fact that a desirable MMW output power can be obtained with a much smaller PD photocurrent under optical short pulse excitation [23]. Although the optical pulse train should result in the harmonic of the photo-generated MMW signal from PDs, it can be easily filtered out due to the limited bandwidth of transmitter and receiver in a communication system, especially when the repetition rate of optical pulse reaches the MMW regime ($>$ 100 GHz). Such a pulse train can thus be used as the single-frequency sinusoidal MMW carrier signal with a larger ($>$ 100%) modulation depth. It is interesting to note a demonstration for the 10 GHz range has been reported in the same vein [24]. The main drawback of such a short pulse excitation over a long fiber link is then dispersion management (typically using dispersion compensating fiber) becomes pivotal [25]. Recently, such a high-modulation-depth photonic MMW carrier has been provided by time-multiplexing a mode-locked laser output to generate short optical pulses with 120 GHz repetition rate [23]. The modulation depth of such a signal increases as the duration of the optical pulse decreases, resulting in a 4.3 dB MMW output power enhancement, as compared with conventional sinusoidal excitation.

In Section 2 of this paper, a theoretical analysis on the MMW spectral power enhancement enabled using optical short pulses comprised of equi-amplitude frequency components is presented. We will show that a moderately short (picosecond) pulse can provide a comparable MMW power enhancement as to that by an ultrashort (femtosecond) pulse. This result is favorable in alleviating dispersion and other nonlinear effects in fiber transmission of femtosecond pulses. In Section 3, a single line-by-line pulse shaper is used to optimize the output of a phase-modulated continuous-wave (PMCW) laser frequency comb [26], [27] for simultaneous generation of ultrahigh-rate W-band signals and dispersion precompensation. In Section 4, a high-power flip-chip bonded near-ballistic uni-traveling-carrier photodiode (NBUTC-PD) [28] is excited using the shaper-optimized W-band waveform generator to accomplish a 7.4 dB spectral power enhancement at 100 GHz. Compared with that reported in [23], we have achieved higher power enhancement (7.4 dB versus 4.3 dB) by using a broader optical pulse duration (2.6 ps versus $<$ 1 ps). In addition, through different pulse shaper settings, the optical pulse duration, repetition rate, and peak power are varied, and distinct nonlinear behaviors of NBUTC-PD are experimentally demonstrated. These nonlinear characteristics can be attributed to the near-ballistic transport of photo-generated electrons [29], [30] and the space-charge screening effect [31], which originates from the high-peak output voltage of photo-generated electrical pulses.

2. Theoretical Analysis

We first present a theoretical analysis over the potential of MMW spectral power enhancement using pulsed versus sinusoidal excitation. We assume that a fixed average optical power, for either types of the excitation, is used to yield a constant average current from the PD. It is well known that the PD current $i_{PD}(t)$ can be expressed as $i_{PD}(t) = g(t) \otimes P(t)$, where $g(t)$ is the linear detector impulse response, $P(t)$ is the optical power, and $\otimes$ denotes convolution. In this study, the MMW spectral power enhancements are measured using an electrical spectrum analyzer (ESA). An ESA measures the current power spectrum $|\tilde{I}_{PD}(\omega)|^2$ defined as $|\tilde{I}_{PD}(\omega)|^2 = |\tilde{G}(\omega) \cdot \tilde{P}(\omega)|^2$, where $\tilde{G}(\omega)$
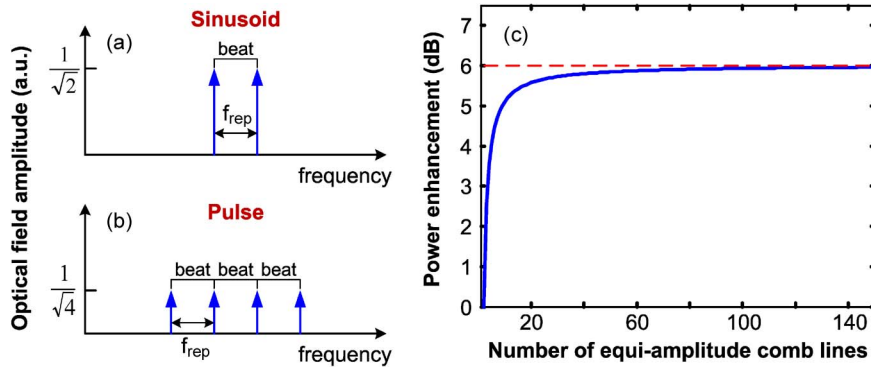
Fig. 1. Schematic of the optical field amplitudes for (a) a time-domain sinusoid and (b) a time-domain pulse. (c) Result of theoretical MMW spectral power enhancements at f_{rep} with respect to the number of equi-amplitude comb lines.

and $\widetilde{P}(\omega)$ denote the base-band frequency spectra of $g(t)$ and $P(t)$ through the Fourier-Transform relation, respectively.

Without loss of generality, two assumptions are further made to facilitate our analysis: 1) All frequency components (hereafter referred as comb lines) have equal amplitude, and 2) all of the comb lines are in phase. The second assumption, which is known as the transform-limited condition, gives the shortest pulse obtainable for a given frequency spectrum. We first look at the sinusoidal excitation, as depicted in Fig. 1(a). A time-domain sinusoid is equivalent to having two distinct comb lines with equal optical field amplitude. Here, we assume a normalized average optical power of $P_{avg} = 1$, therefore each frequency comb line acquires an amplitude of $1/\sqrt{2}$. The frequency spacing f_{rep} (pulse repetition frequency) between the two lines is related to the temporal period T of the sinusoid through $f_{rep} = 1/T$. We now emphasize on the MMW spectral power at the fundamental frequency $|\widetilde{I}_{PD}(2\pi f_{rep})|^2 \propto |\widetilde{P}(2\pi f_{rep})|^2$. The value of $|\widetilde{P}(2\pi f_{rep})|$ can be obtained through the sum of beatings between every two comb lines. For the sinusoidal case, only one beat value can be obtained. One can therefore express the spectral power coefficient at f_{rep} under sinusoidal excitation as $|\widetilde{P}_{\sin}(2\pi f_{rep})|^2 = ((1/\sqrt{2}) \cdot (1/\sqrt{2}))^2 = 1/4$.

We now focus on the pulsed excitation case (higher temporal modulation depth), which is represented in Fig. 1(b) using four equi-amplitude comb lines. To hold our basic condition for a fixed average optical power of $P_{avg} = 1$, each frequency comb line now has a normalized amplitude of $1/\sqrt{4}$. For this four-line pulsed excitation, three equal beatings exist, and the spectral power coefficient at f_{rep} is evaluated as $|\widetilde{P}_{4-line}(2\pi f_{rep})|^2 = [((1/\sqrt{4}) \cdot (1/\sqrt{4})) \cdot 3]^2 = 9/16$. An ideal MMW spectral power-enhancement factor at the fundamental pulse repetition frequency for the four-line pulse excitation referenced to sinusoidal excitation can be therefore formulated as

$$\eta_4(f_{rep}) \equiv \frac{\left|\widetilde{P}_{4-line}(2\pi f_{rep})\right|^2}{\left|\widetilde{P}_{\sin}(2\pi f_{rep})\right|^2} = \frac{9}{4}. \tag{1}$$

In analogy for the derivation for (1), a generalized MMW spectral power-enhancement factor can be derived for an optical pulse comprised of N comb lines with equal amplitudes of $1/\sqrt{N}$ as

$$\eta_N(f_{rep}) \equiv \frac{\left|\widetilde{P}_{N-line}(2\pi f_{rep})\right|^2}{\left|\widetilde{P}_{\sin}(2\pi f_{rep})\right|^2} = \frac{\left(\frac{N-1}{N}\right)^2}{1/4} = 4\left(1 - \frac{1}{N}\right)^2. \tag{2}$$

Equation (2) is plotted as a function of number of comb lines N in semi-log scale in Fig. 1(c). It is interesting to note from our simplified derivation, in the limiting case of a very short pulse (N approaching infinity), a maximum of 6 dB spectral power-enhancement factor is obtained as
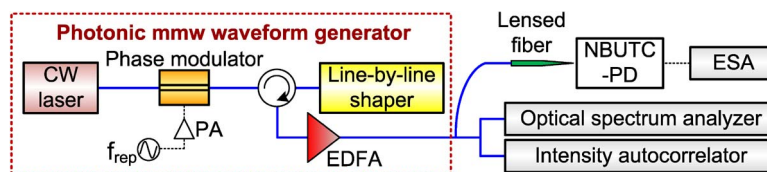
Fig. 2. Schematic of the experimental setup. PA: power amplifier; EDFA: erbium-doped fiber amplifier; NBUTC-PD: near-ballistic uni-traveling carrier photo-diode; ESA: electrical spectrum analyzer.

compared with using a sinusoidal excitation onto a PD. Our finding indicates that a moderately short pulse is capable of producing a MMW power enhancement that is comparable with that by a delta-like pulse. This finding is especially significant since dispersion and other optical nonlinearities are less detrimental for a broader pulse. Our analysis can be used to explain the results reported in [23] and [24].

3. Experimental Setup

Fig. 2 shows the schematic of our experimental setup. A PMCW laser frequency comb is generated by injecting a narrow-linewidth CW laser (NKT Adjustik, 1545 nm) into a low-V_π LiNbO$_3$ phase modulator (EO Space, with $V_\pi \sim 2.8$ V at 1 GHz). A 20 GHz sinusoidal signal from an ultralow phase noise RF signal generator (Agilent E8257D), amplified to $+30$ dBm, is used to drive the phase modulator. The phase modulation frequency of 20 GHz equals the resulting frequency comb line spacing [26], [27]. The generated 20 GHz comb is sent to a home-made fiber-coupled reflective line-by-line pulse shaper for independent phase/amplitude control.

The details of our line-by-line shaper are as follows: A fiber-pigtailed collimator with a 3.5 mm spot diameter is used to send the comb onto a 1200 grooves/mm gold-coated grating. Discrete comb lines are diffracted by the grating and focused by a lens with a 500 mm focal length. A fiberized polarization controller is used to adjust for horizontal polarization on the grating. A computer controllable 2 $\times$ 640 pixel liquid crystal modulator (LCM, CRI SLM-640-D-NM) array is placed just before the focal plane of the lens to independently control both amplitude and phase of individual spectral lines. A retro-reflecting mirror placed on the rear focal plane (the Fourier plane) of the lens leads to a double-pass geometry, with all the spectral lines recombined into a single fiber and separated from the input via an optical circulator. The LCM layers with liquid crystal axis configured as $+/-45°$ introduce phase shift and, thus, modify polarizations of input light. Combined with a polarizer placed between the collimator and the grating, gray-level intensity control can be achieved with maximum extinction ratio up to ~25 dB by the LCM. The fiber-to-fiber insertion loss of the pulse shaper is 7.4 dB (including circulator loss), which includes all optical component losses, as well as loss incurred in focusing back into the 9 μm fiber mode after the pulse shaper.

An erbium-doped fiber amplifier (EDFA) is used after the pulse shaper to provide variable optical power launched to our device. Fifty percent of the EDFA output is coupled into our device-under-test (DUT) through a lensed fiber. Our DUT is an NBUTC-PD module with a wide optical-to-electrical bandwidth (> 110 GHz) and a saturation current as high as 37 mA [28]. The whole module is flip-chip bonded on an AlN substrate for enhanced heat-sinking under high-power operation. The photo-generated MMW power from the DUT is recorded by a W-band power sensor head (Agilent W8486A) or ESA (Agilent E4448A) with an external W-band mixer (Agilent 11970W). The other 50% of the EDFA output is directed to either an optical spectrum analyzer (OSA) or a home-made noncollinear intensity autocorrelator for optical characterizations.

Fig. 3 shows the experimental optical spectra and the corresponding waveforms from the line-by-line shaper output. Fig. 3(a) shows the optical spectrum of the initial 20 GHz spacing frequency comb after spectral phase optimization. We demonstrate comb line spacing conversion using shaper amplitude control, resulting in either a two-line (see Fig. 3(b): two lines spaced 100 GHz apart with side-mode suppression ratio (SMSR, which is limited by the LCM polarization extinction ratio) greater than 25 dB for sinusoidal waveform in the time-domain) or four-line (see Fig. 3(c):
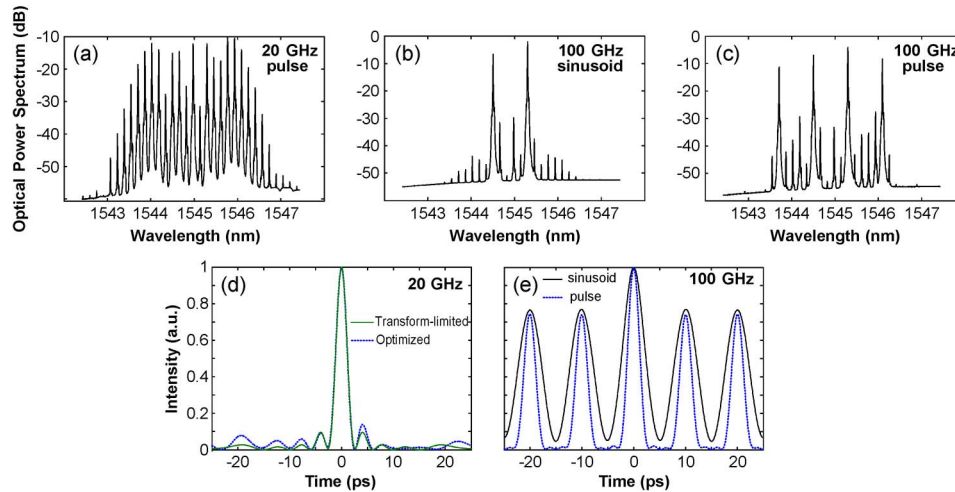
Fig. 3. Measured optical spectra of (a) 20 GHz, (b) 100 GHz two-line, and (c) 100 GHz four-line combs. (d) 20 GHz transform-limited pulse (solid) and the waveform optimized for maximum MMW power generation (dot). (e) Time-domain intensities of the 100 GHz two-line and the four-line waveforms optimized for maximum MMW power.

generating pulses in the time-domain) output comb spectra with 100 GHz line spacing. The four-line comb at 100 GHz spacing is capable of providing shorter optical pulse duration, as compared with the two-line sinusoidal case; thus, a higher MMW output power from our DUT can be anticipated under the same operating current from our theoretical prediction.

The procedures used to derive the shaper-optimized optical waveforms are described as follows: 1) Intrinsically, the spectral phase of a PMCW laser frequency comb exhibits abrupt phase jumps from one comb line to the next and giving a constant (CW) time-domain intensity profile [26], [27]. Therefore, in order to generate transform-limited pulses in the time-domain out of the initial 20 GHz PMCW comb, a desired spectral phase correction setting $\Phi_0(\omega)$ needs to be applied onto the comb lines to obtain flat spectral phase condition. This is achieved by applying phase control to each comb line through an automated process via maximizing the second-harmonic yield of a noncollinear intensity autocorrelator positioned at zero delay [14]. This procedure also ensures the compensation of the slight residual quadratic phase of the pulse shaper. 2) We then direct the optical pulses onto our DUT. With the slightly added fiber length as well as the dispersion relation of the lensed-fiber, intuitively spectral phase precompensation is required for delivery of the pulses onto the DUT. For each amplitude control case, we obtain an optimized spectral phase precompensation setting $\Phi_i(\omega)$ through phase control to the unblocked comb lines by maximizing the photo-generated MMW power from our DUT using the automated process. 3) By applying the phase difference between $\Phi_i(\omega)$ and $\Phi_0(\omega)$ onto the experimental optical spectra, we are able to determine the corresponding optimized waveform for each frequency comb spectrum exiting the pulse shaper.

Fig. 3(d) shows the time-domain intensities of the 20 GHz transform-limited (solid trace, with full-width half-maximum (FWHM) duration of 2.5 ps) and the pulse for maximum MMW power generations (dotted trace). The MMW power optimized waveforms show only a slight deviation from the transform-limited pulse, which we attribute to the extra dispersion caused by the fiber link and the lensed fiber. Fig. 3(e) shows the optical waveforms for the 100 GHz sinusoidal and the four-line pulses. Due to finite shaper extinction ratio, the 100 GHz waveforms show a 20 GHz intensity envelope and affect the resulting RF signal purity. Detailed discussions over this issue will be addressed in Section 4. As can be seen, the FWHM duration of optical pulse can be shortened from 4.8 ps to around 2.6 ps when the number of optical comb lines increase from two to four. Compared with the results shown in Fig. 3(d), the duration of the 100 GHz optical pulse is almost identical since the total optical bandwidth remains comparable.
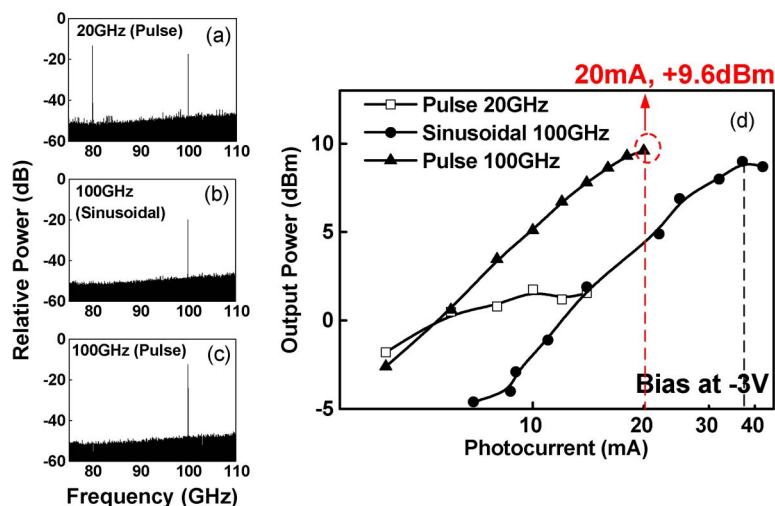
Fig. 4. Measured MMW spectra of (a) 20 GHz optical pulse train, (b) 100 GHz sinusoid, and (c) 100 GHz optical pulse train. (d) Measured photo-generated MMW power at W-band versus photocurrent under the three optical excitation schemes.

4. Result and Discussion

Fig. 4(a)–(c) shows the measured W-band power spectra corresponding to 20 GHz optical pulse train, 100 GHz sinusoid, and 100 GHz optical pulse train, respectively. In Fig. 4(a), there are two tones (80 and 100 GHz), corresponding to fourth and fifth harmonic of the 20 GHz signal. For 100 GHz sinusoidal and pulse excitation, as shown in Fig. 4(b) and (c), only one tone at 100 GHz is observed due to limited bandwidth (110 GHz) of our instrument. Fig. 4(d) shows the measured photo-generated MMW power at W-band versus output photocurrent under the three types of optical excitations investigated. The DUT was reverse biased at -3 V. The losses of the microwave probe, bias tee, and cables at 100 GHz during measurement have been deembedded carefully ($\sim$9 dB total at 100 GHz). As can be seen, excitation with the 20 GHz optical pulse train (squares) resulted in the worst performance among the three excitation schemes, generating the lowest output power and the smallest saturation power. This is reasonable since a majority of the MMW power spectral components (20, 40, and 60 GHz) generated by the 20 GHz pulse train do not fall within the W-band and, thus, are not detected. In addition, the peak power of the 20 GHz pulse train is roughly five times higher than that of the 100 GHz optical signal under the same averaged photocurrent operation. This leads to a much lower saturation current due to high peak output electrical field from PD and its induced space-charge screening effect [31].

On the other hand, the output power generated by 100 GHz optical pulse train excitation [filled triangles in Fig. 4(d)] is 7.4 dB higher than that achieved by 100 GHz sinusoidal excitation under the same photocurrent. Although the 100 GHz pulse operation shows a lower saturation current (20 mA) than that of sinusoidal excitation (37 mA), it exhibits a higher maximum saturation MMW power (9.6 versus 9 dBm). These results clearly indicate that by using the optimized 100 GHz optical pulse train, our device can generate the desired output MMW power in the W-band under a much smaller (around half) output photocurrent than that under sinusoidal operation. This implies an extended device lifetime, enhanced reliability, and lower optical power budget for system operation. One of the reasons leading to our observed enhancement in output MMW power is due to the presence of two more additional optical comb lines, as shown in Fig. 3(b) and (c). A larger 100 GHz beat signal is obtained when more optical comb lines are all in phase. Based on the measured optical power spectra, we have derived a theoretical improvement of 5.6 dB. The 1.8 dB discrepancy (5.6 versus 7.4 dB improvement experimentally obtained) is tentatively attributed to the phenomenon of near-ballistic transport of photo-generated electrons [32], [33] in our NBUTC-PD and will be discussed further in the next paragraph. Furthermore, our shaper-assisted MMW waveforms can achieve a
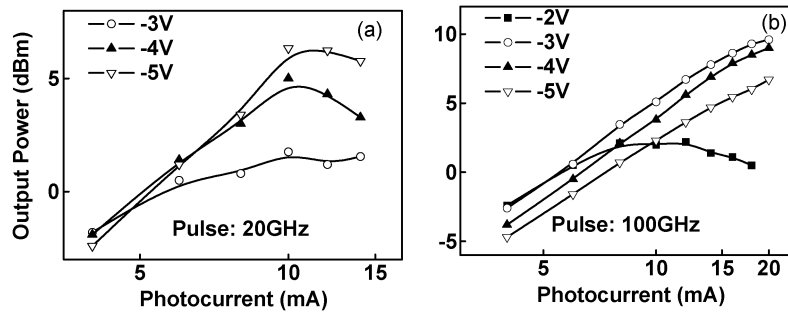
Fig. 5. Measured bias-dependent MMW power versus photocurrent under (a) 20 and (b) 100 GHz pulse excitations.

larger improvement in modulation depth (7.4 versus 4.3 dB), as compared with the reported value in previous work [23] by use of a mode-locked laser with a sub-picosecond optical pulse train. The dispersion effect in fiber transmission is an important issue for remote distribution of a high-frequency ($\sim$100 GHz) optical local-oscillator (LO) signal [25]. The present approach is also advantageous in this respect as a much broader optical pulse-width (2.6 ps versus < 1 ps) can be used. Furthermore, using the optical pulse shaper, the spectral phase of the optical pulse can be precompensated to obtain better photo-generated MMW power performance, as opposed to optical pulses generated directly from mode-locked lasers.

Here, we provide a discussion over the resulting RF signal purity limited by the shaper extinction ratio. Although filtered by the NBUTC-PD, there should still be residual RF signals at 20, 40 and 60 GHz due to the unsuppressed comb lines as shown in Fig. 3(b) and (c). Without loss of generality, here, we focus on the 20 GHz RF signal power level. From Fig. 3(b) and (c), we have calculated the residual RF power level at 20 GHz (normalized to that at 100 GHz) to be −21.62 dBc for the two-comb-line case [see Fig. 3(b)], and −23.32 dBc for the four-comb-line case [see Fig. 3(c)], respectively. As commercial LCM with higher polarization extinction ratio may not be readily available, the signal purity can be improved currently by cascading multiple identical pulse shapers. By assuming an equi-amplitude frequency comb, the residual 20 GHz RF power level can be further suppressed down to −43.94 (−68.98) dBc if two (three) identical shapers are cascaded to obtain an overall 50 (75) dB SMSR values, respectively.

Fig. 5(a) and (b) shows the measured bias-dependent MMW power versus photocurrent under 20 and 100 GHz pulse excitations, respectively. In Fig. 5(a), the maximum output MMW power and the saturation current increased significantly as the reverse bias voltage was ramped up to −5 V. Such effect can be understood by noting that a higher reverse bias voltage is required in compensating the high peak output electrical field and minimizing the space-charge screening effect [31]. On the other hand, an optimal reverse bias voltage of −3 V is observed under 100 GHz optical pulse excitation as shown in Fig. 5(b). Higher reverse bias voltages (−4 V and −5 V) result in degraded output power. We note further that the optical peak powers of 100 GHz optical pulses are around one fifth of that of the 20 GHz pulse, under the same averaged photocurrent operation. This leads to less serious peak-electrical-field-induced space-charge screening effect for the former case. The optimal bias voltage (−3 V) under 100 GHz pulse excitation may correspond to the required electrical field inside the collector layer of NBUTC-PD to sustain an overshoot drift-velocity of electrons [32], [33]. A higher electron drift-velocity in turn means a larger RF current and output power [29], [30]. When the reverse bias voltage reaches −5 V, the electrical field in the collector layer would then be too high to sustain an overshoot drift-velocity. As a result, we observe the degradation in output MMW power. The same behavior has been reported for UTC-PD [30] with a much lower optimal reveres bias voltage than that of NBUTC-PD (−0.75 V versus −3 V). Such a small optimum reverse bias (<−1 V) limits the maximum saturation current of PD [30] as the carriers are easily screened by the output RF voltage on a 50 Ω load [31]. By inserting an additional p-doped layer inside the collector layer of the NBUTC-PD to redistribute the electrical field [28], [32], [33], we have demonstrated here that the optimal bias can indeed be increased to −3 V. The

aforementioned problem is effectively eliminated. In addition, compared with NBUTC-PD under pure sinusoidal signal excitation [28], [32], [33], the observed degradation in output RF power under high reverse bias (-5 V) is much less severe here. The highly nonlinear velocity over-shot phenomena in the DUT may be responsible for the observed 1.8 dB higher output RF power than the theoretical prediction. We recall that our analysis on RF output enhancement was based on linear response of the PD.

5. Conclusion

We experimentally demonstrate a single line-by-line optical pulse shaper that is capable of providing simultaneous high-modulation-depth photonic MMW waveform generations and dispersion precompensation. Compared with the pure sinusoidal optical MMW signal at 100 GHz, a 7.4 dB improvement in modulation depth is observed using 2.6 ps pulse excitation. The superior modulation-depth (7.4 dB versus 4.3 dB) performance of the reported optical pulse train with a close repetition rate (120 GHz) and narrower pulse-width (< 1 ps versus 2.6 ps) from a mode-locked laser is attributed to our capability in performing line-by-line control in obtaining maximized W-band MMW power and the distinct nonlinear behavior of NBUTC-PD itself. A theoretical analysis on MMW power enhancement using pulsed excitation is presented and is in good qualitative agreement with our experimental results. Using such novel optical source, distinct nonlinear behaviors originating from space-charge screening effect and over-shoot drift-velocity of electrons in NBUTC-PD under different reverse bias voltages, photocurrents, and optical pulse repetition rates (20 and 100 GHz) are experimentally observed.

Acknowledgment

References

[1] J. Capmany and D. Novak, "Microwave photonics combines two worlds," *Nat. Photon.*, vol. 1, no. 6, pp. 319–330, Jun. 2007.

[2] J. Yao, "Microwave photonics," *J. Lightw. Technol.*, vol. 27, no. 3, pp. 314–335, Feb. 2009.

[3] P. J. Delfyett, S. Gee, M.-T. Choi, H. Izadpanah, W. Lee, S. Ozharar, F. Quinlan, and T. Yilmaz, "Optical frequency combs from semiconductor lasers and applications in ultrawideband signal processing and communications," *J. Lightw. Technol.*, vol. 24, no. 7, pp. 2701–2719, Jul. 2006.

[4] A. M. Weiner, "Femtosecond pulse shaping using spatial light modulators," *Rev. Sci. Instrum.*, vol. 71, no. 5, pp. 1929–1960, May 2000.

[5] A. M. Weiner, "Manipulation of ultrashort pulses," in *Ultrafast Optics*. Hoboken, NJ: Wiley, 2009, pp. 362–421.

[6] J. D. McKinney, D. E. Leaird, and A. M. Weiner, "Millimeter-wave arbitrary waveform generation with a direct space-to-time pulse shaper," *Opt. Lett.*, vol. 27, no. 15, pp. 1345–1347, Aug. 2002.

[7] J. Chou, Y. Han, and B. Jalali, "Adaptive RF-photonic arbitrary waveform generator," *IEEE Photon. Technol. Lett.*, vol. 15, no. 4, pp. 581–583, Apr. 2003.

[8] J. D. McKinney, I. S. Lin, and A. M. Weiner, "Shaping the power spectrum of ultra-wideband radio-frequency signals," *IEEE Trans. Microw. Theory Tech.*, vol. 54, no. 12, pp. 4247–4255, Dec. 2006.

[9] I. S. Lin, J. D. McKinney, and A. M. Weiner, "Photonic synthesis of broadband microwave arbitrary waveforms applicable to ultra-wideband communication," *IEEE Microw. Wireless Compon. Lett.*, vol. 15, no. 4, pp. 226–228, Apr. 2005.

[10] H. Chi, F. Zeng, and J. Yao, "Photonic generation of microwave signals based on pulse shaping," *IEEE Photon. Technol. Lett.*, vol. 19, no. 9, pp. 668–670, May 2007.

[11] M. H. Khan, H. Shen, Y. Xuan, L. Zhao, S. Xiao, D. E. Leaird, A. M. Weiner, and M. Qi, "Ultrabroad-bandwidth arbitrary radiofrequency waveform generation with a silicon photonic chip-based spectral shaper," *Nat. Photon.*, vol. 4, no. 2, pp. 117–122, Feb. 2010.

[12] Z. Jiang, D.-S. Seo, D. E. Leaird, and A. M. Weiner, "Spectral line-by-line pulse shaping," *Opt. Lett.*, vol. 30, no. 12, pp. 1557–1559, Jun. 2005.

[13] J. Ye and S. T. Cundiff, Eds., *Femtosecond Optical Frequency Comb: Principle, Operation, and Applications*. New York: Springer-Verlag, 2005.

[14] Z. Jiang, C.-B. Huang, D. E. Leaird, and A. M. Weiner, "Optical arbitrary waveform processing of more than 100 spectral comb lines," *Nat. Photon.*, vol. 1, no. 8, pp. 463–467, Aug. 2007.

[15] N. K. Fontaine, R. P. Scott, J. Cao, A. Karalar, W. Jiang, K. Okamoto, J. P. Heritage, B. H. Kolner, and S. J. B. Yoo, "32 phase X 32 amplitude optical arbitrary waveform generation," *Opt. Lett.*, vol. 32, no. 7, pp. 865–867, Apr. 2007.

[16] C.-B. Huang, D. E. Leaird, and A. M. Weiner, "Time-multiplexed photonically enabled radio-frequency arbitrary waveform generation with 100 ps transitions," *Opt. Lett.*, vol. 32, no. 22, pp. 3242–3244, Nov. 2007.

[17] C.-B. Huang, D. E. Leaird, and A. M. Weiner, "Synthesis of millimeter-wave power spectra using time-multiplexed optical pulse shaping," *IEEE Photon. Technol. Lett.*, vol. 21, no. 18, pp. 1287–1289, Sep. 2009.

[18] C.-B. Huang and A. M. Weiner, "Analysis of time-multiplexed optical line-by-line pulse shaping: Application for radio-frequency and microwave photonics," *Opt. Express*, vol. 18, no. 9, pp. 9366–9377, Apr. 2010.

[19] J. Wells, "Faster than fiber: The future of multi-Gb/s wireless," *IEEE Microw. Mag.*, vol. 10, no. 3, pp. 104–112, May 2009.

[20] A. Hirata, H. Takahashi, R. Yamaguchi, T. Kosugi, K. Murata, T. Nagatsuma, N. Kukutsu, and Y. Kado, "Transmission characteristics of 120-GHz-band wireless link using radio-on-fiber technologies," *J. Lightw. Technol.*, vol. 26, no. 15, pp. 2338–2344, Aug. 2008.

[21] F.-M. Kuo, J.-W. Shi, S.-N. Wang, N.-W. Chen, P.-T. Shih, C.-T. Lin, W.-J. Jiang, E.-Z. Wong, J. Chen, and S. Chi, "W-band wireless data transmission by the integration of a near-ballistic uni-traveling-carrier photodiode (NBUTC-PD) with a horn antenna fed by a quasi-Yagi radiator," *IEEE Electron Device Lett.*, vol. 30, no. 11, pp. 1167–1169, Nov. 2009.

[22] J. Lee, Y. Huang, Y. Chen, H. Lu, and C. Chang, "A low-power fully integrated 60 GHz transceiver system with OOK modulation and on-board antenna assembly," in *Proc. Dig. Int. Solid-State Circuits Conf.*, 2009, pp. 316–317.

[23] A. Hirata, M. Harada, and T. Nagatsuma, "120-GHz wireless link using photonic techniques for generation, modulation, and emission of millimeter-wave signals," *J. Lightw. Technol.*, vol. 21, no. 10, pp. 2145–2153, Oct. 2003.

[24] S. A. Diddams, M. Kirchner, T. Fortier, D. Braje, A. M. Weiner, and L. Hollberg, "Improved signal-to-noise ratio of 10 GHz microwave signals generated with a mode-filtered femtosecond laser frequency comb," *Opt. Express*, vol. 17, no. 5, pp. 3331–3340, Mar. 2009.

[25] C.-W. Chow, F.-M. Kuo, J.-W. Shi, C.-H. Yeh, Y.-F. Wu, C.-H. Wang, Y.-T. Li, and C.-L. Pan, "100 GHz ultra-wideband (UWB) fiber-to-the-antenna (FTTA) system for in-building and in-home networks," *Opt. Express*, vol. 18, no. 2, pp. 473–478, Jan. 2010.

[26] C.-B. Huang, S.-G. Park, D. E. Leaird, and A. M. Weiner, "Nonlinearly broadened phase-modulated continuous-wave laser frequency combs characterized using DPSK decoding," *Opt. Express*, vol. 16, no. 4, pp. 2520–2527, Feb. 2008.

[27] C.-B. Huang, Z. Jiang, D. E. Leaird, and A. M. Weiner, "High-rate femtosecond pulse generation via line-by-line processing of a phase-modulated CW laser frequency comb," *Electron. Lett.*, vol. 42, no. 19, pp. 1114–1115, Sep. 2006.

[28] J.-W. Shi, F.-M. Kuo, C.-J. Wu, C. L. Chang, C. Y. Liu, C.-Y. Chen, and J.-I. Chyi, "Extremely high saturation current-bandwidth product performance of a near-ballistic uni-traveling-carrier photodiode with a flip-chip bonding structure," *IEEE J. Quantum Electron.*, vol. 46, no. 1, pp. 80–86, Jan. 2010.

[29] H. Ito, S. Kodama, Y. Muramoto, T. Furuta, T. Nagatsuma, and T. Ishibashi, "High-speed and high-output InP-InGaAs unitraveling-carrier photodiodes," *IEEE J. Sel. Topics Quantum Electron.*, vol. 10, no. 4, pp. 709–727, Jul./Aug. 2004.

[30] H. Ito, T. Furuta, F. Nakajima, K. Yoshino, and T. Ishibashi, "Photonic generation of continuous THz wave using uni-traveling-carrier photodiode," *J. Lightw. Technol.*, vol. 23, no. 12, pp. 4016–4021, Dec. 2005.

[31] P.-L. Liu, K.-J. Williams, M. Y. Frankel, and R. D. Esman, "Saturation characteristics of fast photodetectors," *IEEE Trans. Microw. Theory Tech.*, vol. 47, no. 7, pp. 1297–1303, Jul. 1999.

[32] Y.-S. Wu, J.-W. Shi, and P.-H. Chiu, "Analytical modeling of a high-performance near-ballistic uni-traveling-carrier photodiode at a 1.55 μm wavelength," *IEEE Photon. Technol. Lett.*, vol. 18, no. 8, pp. 938–940, Apr. 2006.

[33] Y.-S. Wu and J.-W. Shi, "Dynamic analysis of high-power and high-speed near-ballistic unitraveling carrier photodiodes at W-band," *IEEE Photon. Technol. Lett.*, vol. 20, no. 13, pp. 1160–1162, Jul. 2008.